Plots of k_{ET} vs. T are shown in Figure 8. At high temperatures a more or less exponential relationship is observed. The values for k_{ET} ($T \rightarrow \infty$) and ΔE, determined from this region, are contained in Table IV. They have to be considered as a lower limit to the true activation energy. The reason for the deviations from an Arrhenius type behavior at low temperatures lies in the dominance of alternative processes with very low activation barriers. One likely possibility are transfer processes to the killer traps from their near Ni^{2+} neighbors. The overall transfer rate k_{ET} from the nickel system to the quenching traps may be limited by the individual $Ni^{2+} \rightarrow Ni^{2+}$ steps, i.e. diffusion within the Ni^{2+} system, or the trapping step may be limiting. Our data do not allow a clear assignment to one of these limiting cases, because the nature of the killer traps is not known. However, an activation barrier is expected for the $Ni^{2+} \rightarrow Ni^{2+}$ step on several grounds. Resonant energy transfer depends on the spectral overlap between the donor emission and acceptor absorption bands. As a result of the geometrical expansion in the relaxed excited state and the concomitant Stokes shift, only the very weak electronic origins contribute to the spectral overlap below 10 K. This would be the most obvious reason for a thermal activation of the $Ni^{2+} \rightarrow Ni^{2+}$ transfer. In antiferromagnetically ordered materials, and there are antiferromagnetic correlations along the chains in $CsNiX_3$ type compounds up to high temperatures,[34] there is an additional barrier. Excitation transfer between nearest neighbors is doubly spin-forbidden. This can be overcome by magnon-assisted processes, which require finite magnon populations and thus lead to a thermal activation. Finally, the trigonal ^3E_g (T_{2g}) component may be highly more efficient to promote purely excitonic energy transfer than $^3A_{1g}$ (T_{2g}), which again would lead to a thermally activated process. This mechanism was recently postulated to be mainly responsible for the energy-transfer behavior in several antiferromagnetic Mn^{2+} compounds.[35] The observed activation energies in $CsNiCl_3$ and $CsNiBr_3$ are similar in magnitude to those determined in $[(CH_3)_4N]MnCl_3$,[36] $RbMnCl_3$, and $CsMnBr_3$.[35] Relaxation in the excited state and transfer via a high-energy exciton are both likely mechanisms for the observed thermal barriers in the Ni^{2+} systems.

Acknowledgment. We thank H. Riesen for helpful discussions. Financial support by the Swiss National Science Foundation is gratefully acknowledged.

Registry No. $CsNiCl_3$, 15455-69-3; $CsNiBr_3$, 15455-70-6.

(34) Ueda, K.; Tanabe, Y. *J. Phys. Soc. Jpn.* **1980**, *48*, 1137.
(35) Kambli, U.; Güdel, H. U. *Inorg. Chem.* **1984**, *23*, 3479.
(36) Yamamoto, H.; McClure, D. S.; Marzzacco, C.; Waldman, M. *Chem. Phys.* **1977**, *22*, 79.

Contribution from the Departments of Chemistry, Ben Gurion University, Beer Sheva 84120, Israel, and North Carolina State University, Raleigh, North Carolina 27695-8204

Electronic and Intramolecular Structural Localizations in Conducting Organic Salts

Sason S. Shaik*[†] and Myung-Hwan Whangbo*[‡]

Received June 24, 1985

We examined the energy factors governing intramolecular structural localization, which leads to a mixed-valence structure for molecular stacks and hence to a $4k_f$ CDW in small-U limit (i.e., $U/4|\beta| < 1$). Intramolecular structural localization is found to occur when $E_R/4|\beta| > 1$, where the intramolecular relaxation energy E_R is a measure of the tendency for a stacking molecule to relax its geometry upon losing or gaining an electron. For a donor stack E_R is found to be approximated by $2(IP^v - IP^a)$, given the vertical and adiabatic ionization potentials of the donor as IP^v and IP^a, respectively. On the basis of these ionization potentials and the estimates of bandwidth $4|\beta|$, the intramolecular structural localization condition was tested for several well-studied organic salts. For a donor molecule, the tendency for intramolecular relaxation is found to increase as antibonding character of its HOMO increases. Thus, sulfur-based donor molecules have a stronger tendency for intramolecular relaxation than do their selenium analogues, which appears to be why a $4k_f$ CDW is more likely to be found from sulfur-based donors. To examine how electronic localization (i.e., $U/4|\beta| > 1$) and intramolecular structural localization (i.e., $E_R/4|\beta| > 1$) affect the electronic structures of molecular stack, we performed band electronic structure calculations on several mono-valence and mixed-valence structures of $TTF^{1/2+}$ and $TTF^{2/3+}$ stacks. Analysis of these results led us to formulate simple models of $2k_f$ and $4k_f$ CDW's in terms of intramolecular and intermolecular distortions.

In the past decade, conducting organic salts have been synthesized from various donor and acceptor molecules (e.g., see Chart I).[1] Invariably, these organic metals contain stacks of partially oxidized donor molecules D and/or stacks of partially reduced acceptor molecules A. In average, each molecule of a donor or an acceptor stack may be regarded as carrying a fractional charge ρ. For example, $(TMTSF)_2X$ ($X^- = PF_6^-$, ClO_4^-, etc.) is characterized by $TMTSF^{0.5+}$, TTF·TCNQ by $TTF^{0.59+}$ and $TCNQ^{0.59-}$, TSF·TCNQ by $TSF^{0.63+}$ and $TCNQ^{0.63-}$, and $(TTF)_3(BF_4)_2$ by $TTF^{2/3+}$. Many of these organic salts have a metallic conductivity at room temperature but become insulators at lower temperatures owing to some *localization* and *distortion mechanisms* that pin the electrons and restrict their mobility.

Two different mechanisms are generally considered to be responsible for metal–insulator transitions in molecular stacks. One mechanism is a Peierls distortion.[2] In general, a uniform molecular stack with a partially filled metallic band is susceptible to a structural distortion that opens a band gap at the Fermi level. If the band filling is f or $1 - f$ ($0 < f \leq {}^1/_2$), the uniform stack will distort to one in which the unit cell size becomes $1/f$ times as large as that of the uniform stack. An example for such a

Chart I

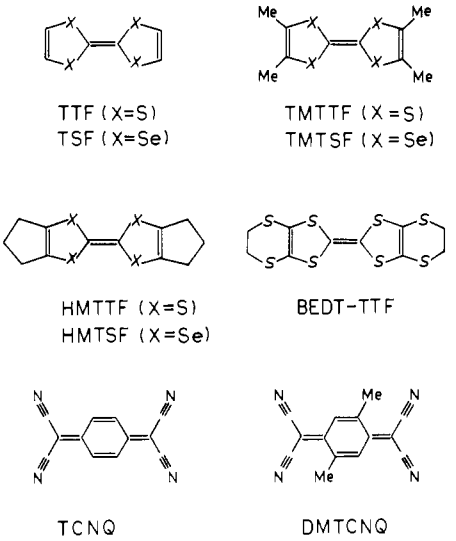

[†] Ben Gurion University.
[‡] Camille and Henry Dreyfus Teacher-Scholar (1980–1985). North Carolina State University.

0020-1669/86/1325-1201$01.50/0

distortion is given by **1a** → **1b**, where a uniform stack $(D^+)_\infty$ with

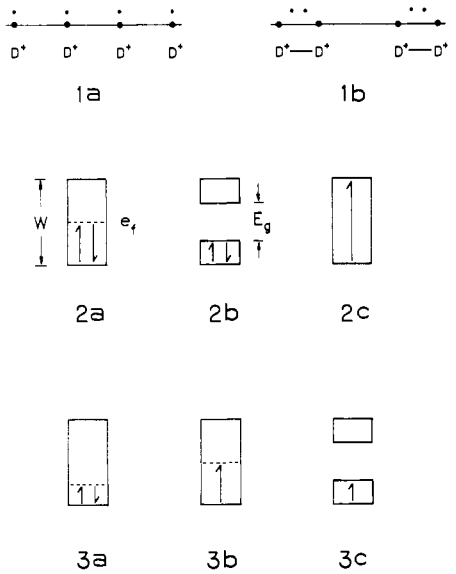

one electron per site ($f = {}^1/_2$) undergoes dimerization. This distortion **1a** → **1b** is accompanied by a change in the band structure from **2a** to **2b** and results in a band gap E_g between the highest occupied and lowest unoccupied band levels. This band gap in **2b** renders the dimerized stack **1b** an insulating material. Such a distortion is classified as a low-spin Peierls ($2k_f$) distortion,[3,4] since it involves transitions between low-spin electronic states. An alternative mechanism of metal–insulator transition is due to electron localization (i.e., formation of unpaired electrons), which originates from electron–electron repulsion.[5] Thus, if the repeat distance of **1a** is large, the resonance integral β is small in magnitude so that the bandwidth W ($=4|\beta|$) becomes small compared with the on-site repulsion U (e.g., electron–electron repulsion that results from two electrons at a given site of **1a**). When $4|\beta| < U$, the metallic state **2a** is less stable than the high-spin state **2c**.[6] This latter state possesses an unpaired electron on each D^+ site of **1a** and is a magnetic insulating state.

When the degree of band filling f is different from ${}^1/_2$, as is the case with most organic metals, electron localization may be accompanied by further structural distortion. Consider for example a uniform molecular stack with a ${}^1/_4$-filled band as in **3a**. If $4|\beta| < U$, the high-spin state **3b** is more stable than the low-spin state **3a**. The state **3b** is further stabilized upon dimerizing the stack, since it leads to another high-spin state **3c** that possesses a band gap. This kind of distortion arising from a band filling f looks as if it were a $2k_f$ distortion of a band filling $2f$ and is classified as a high-spin ($4k_f$) distortion.[3,7] When reference is made to modulations of conduction electron density distribution rather than those of lattice structure, $2k_f$ and $4k_f$ distortions are termed $2k_f$ and $4k_f$ charge density waves (CDW's), respectively.[4,7] Diffuse X-ray- and neutron-scattering studies show that a pseudo-one-dimensional (1D) material can give rise to a $2k_f$ (or $4k_f$) CDW well above the temperature T_c at which a phase transition involving such a CDW occurs (e.g., Peierls phase transition).[4,7] This precursor effect in a 1D system arises from dynamic short-range order: Above T_c ordered domains of a certain average size are created and destroyed as a function of time. As T_c is approached, the average size of ordered domains increases, and eventually the whole system is ordered below T_c (i.e., long-range order).

Therefore, those well-known mechanisms of metal–insulator transition focus upon either *intermolecular* displacive distortion or upon electron localization due to electron–electron repulsion. Yet there exists another mechanism, i.e., electron localization due to intramolecular structural distortion. This may be referred to as *intramolecular structural localization*, which leads to *mixed-valence* structures. Electron localization that occurs in *mono-valence* structures due to electron–electron repulsion may then be referred to as *electronic localization*. Intramolecular structural localization arises from the fact that the optimum geometries of neutral molecules D^0 and A^0 differ from those of charged species D^+ and A^-, respectively. For instance, the $TTF^{2/3+}$ stacks of $(TTF)_3(BF_4)_2$ are made up of TTF^0·TTF^+·TTF^+ triads.[8] Namely, two molecules of each triad adopt the geometry of a fully charged species, and the remaining one adopts that of a neutral species. Likewise, the $TCNQ^{2/3-}$ stacks of $Cs_2(TCNQ)_3$ consist of $TCNQ^0$·$TCNQ^-$·$TCNQ^-$ triads.[9] It is important to note that single-crystal X-ray structure determination provides an "average" structure if a crystal under consideration undergoes fast structural fluctuation arising from dynamic short-range order. Thus, some molecular stacks that appear to have mono-valence structures under the time scale of single-crystal X-ray structural determination may turn out to have mixed-valence structures under the time scale of X-ray photoelectron spectroscopy (XPS).[10] As will

(1) For reviews, see: (a) Williams, J. M. *Prog. Inorg. Chem.* **1985**, *33*, 183. (b) Wudl, F. *Acc. Chem. Res.* **1984**, *17*, 227. (c) Torrance, J. B. *Acc. Chem. Res.* **1979**, *12*, 79. (d) *Ann. N.Y. Acad. Sci.* **1978**, *313*. (e) Hatfield, W. E., Ed. "Molecular Metals"; Plenum Press: New York, 1979. (f) Keller, H. J., Ed. "Chemistry and Physics of One-Dimensional Metals"; Plenum Press: New York, 1977. (g) *J. Phys.* (*Les Ulis, Fr.*) **1983**, *44* (C3), 767–1764. (h) Miller, J. S., Ed. "Extended Linear Chain Compounds"; Plenum Press: New York, 1982–1983; Vol. 1–3. (i) Devreese, J. T., Evrard, R. P., Van Doren, V. E., Eds. "Highly Conducting One-Dimensional Solids"; Plenum Press: New York, 1979.

(2) (a) Peierls, R. E. "Quantum Theory of Solids"; Oxford University Press: London, 1955; p 108. (b) Berlinsky, A. J. *Contemp. Phys.* **1976**, *17*, 331. (c) Whangbo, M.-H. *Acc. Chem. Res.* **1983**, *16*, 95.

(3) Whangbo, M.-H. In "Crystal Chemistry and Properties of Materials with Quasi One-Dimensional Structures"; Rouxel, J., Ed.; Reidel: Dordrecht, The Netherlands, in press.

(4) (a) Comès, R.; Shirane, G. In ref 1i, p 17. (b) Moret, R.; Pouget, J. P. In "Crystal Chemistry and Properties of Materials with Quasi One-Dimensional Structures"; Rouxel, J., Ed.; Reidel: Dordrecht (in press). (c) Jérome, D.; Schulz, H. J. In ref 1h, Vol. 2, p 159. (d) Kobayashi, H.; Kobayashi, A. In ref 1h, Vol. 2, p 259. (e) Kagoshima, S. In ref 1h, Vol. 2, p 303.

(5) (a) Mott, N. F. "Metal-Insulator Transitions"; Barnes & Noble: New York, 1977. (b) Brandow, B. H. *Adv. Phys.* **1977**, *26*, 651. (c) Anderson, P. W. *Solid State Phys.* **1963**, *14*, 99. (d) Hubbard, J. *Proc. R. Soc. London, A* **1963**, *276*, 238. (e) Kanamori, J. *Prog. Theor. Phys.* **1963**, *30*, 275.

(6) (a) Whangbo, M.-H. *J. Chem. Phys.* **1981**, *75*, 4983; **1980**, *73*, 3854; **1979**, *70*, 4963. (b) Whangbo, M.-H. In ref 1h, Vol. 2, p 127.

(7) (a) Pouget, J. P.; Khanna, S. K.; Denoyer, F.; Comès, R.; Garito, A. F.; Heeger, A. J. *Phys. Rev. Lett.* **1976**, *37*, 437. (b) Pouget, J. P.; Comès, R.; Bechgaard, K. In ref 1f, p 113. (c) Pouget, J. P. *Chem. Scr.* **1981**, *17*, 85. (d) Kagoshima, S.; Ishiguro, T.; Anzai, H. *J. Phys. Soc. Jpn.* **1976**, *41*, 2061. (e) Pouget, J. P.; Megtert, S.; Comès, R. In "Recent Developments in Condensed Matter Physics"; Devreese, J. T., Ed.; Plenum: New York, 1981; Vol. 1, p 295. (f) Kagoshima, S.; Anzai, H.; Ishiguro, T.; Engler, E. M.; Schultz, T. D.; Tomkiewicz, Y. In "Lattice Dynamics"; Balkanski, M., Ed.; Flammarion Sciences: Paris, 1978; p 591. (g) Kagoshima, S.; Ishiguro, T.; Engler, E. M.; Schultz, T. D.; Tomkiewicz, Y. *Solid State Commun.* **1980**, *34*, 151. (h) Kagoshima, S.; Pouget, J. P.; Anzai, H. *J. Phys. Soc. Jpn.* **1983**, *52*, 1629.

(8) Legros, J.-P.; Bousseau, M.; Valade, L.; Cassoux, P. *Mol. Cryst. Liq. Cryst.* **1983**, *100*, 181.

(9) (a) Herbstein, F. H. In "Perspectives in Structural Chemistry"; Dunitz, J. D., Ibers, J. A., Eds.; Wiley: New York, 1971; Vol. 4, p 166. (b) Fritchie, C. J., Jr.; Arthur, P., Jr., *Acta Crystallogr.* **1966**, *21*, 139. (c) Arthur, P., Jr., *Acta Crystallogr.* **1964**, *17*, 1176. (d) Enders, H. In ref 1h, Vol. 3, p 263.

(10) (a) Ikemoto, I.; Yamada, M.; Sugano, T.; Kuroda, H. *Bull. Chem. Soc. Jpn.* **1980**, *53*, 1871. (b) Ikemoto, I.; Kikuchi, K.; Yakushi, K.; Kuroda, H. *Solid State Commun.* **1982**, *42*, 257. (c) Ikemoto, I.; Sugano, T.; Kuroda, H. *Chem. Phys. Lett.* **1977**, *49*, 45. (d) Siedle, A. R. In ref 1h, Vol. 2, p 469.

(11) Takahashi, T.; Jérome, D.; Masin, F.; Fabre, J. M.; Giral, L. *J. Phys. C* **1984**, *17*, 3777.

(12) (a) Torrance, J. B.; Silverman, B. D. *Phys. Rev. B: Solid State* **1977**, *15*, 788. (b) Torrance, J. B. *Phys. Rev. B: Condens. Matter* **1978**, *17*, 3099. (c) Lee, P. A.; Rice, T. M.; Klemm, R. A. *Phys. Rev. B: Solid State* **1977**, *15*, 2984. (d) Emery, V. J. *Phys. Rev. Lett.* **1976**, *37*, 107. (e) Kondo, J.; Yamaji, K. *J. Phys. Soc. Jpn.* **1977**, *43*, 424. (f) Hubbard, J. *Phys. Rev. B: Condens. Matter* **1978**, *17*, 494.

(13) Jérome, D.; Schultz, H. J. *Adv. Phys.* **1982**, *31*, 299.

(14) Noguerra, C. *J. Phys. C* **1985**, *18*, 1647.

(15) (a) Heeger, A. J. In ref 1i, p 69. (b) Rybaczewski, E. F.; Smith, L. S.; Garito, A. F.; Heeger, A. J.; Silbernagel, B. G. *Phys. Rev. B: Solid State* **1976**, *14*, 2746. (c) Tomkiewicz, Y.; Taranko, A. R.; Torrance, J. B. *Phys. Rev. B: Solid State* **1977**, *15*, 1017.

be shown later, the tendency for mixed-valence structure occurs when the energy of intramolecular relaxation E_R is large. In other words, the tendency for intramolecular structural localization is enhanced by intramolecular relaxation but diminished by intermolecular resonance interaction. On the other hand, the tendency for electron localization (e.g., **2a** → **2c** or **3a** → **3b**) is enhanced by intramolecular relaxation as well as by electron–electron repulsion but diminished by intermolecular resonance interaction. Therefore, in understanding the electrical and structural properties of organic conducting salts, it is essential to clearly delineate those factors responsible for electronic and intramolecular structural localizations.

Unlike the electronic localization condition (i.e., $U > 4|\beta|$), the intramolecular structural localization condition has received relatively little attention despite the fact that the importance of intramolecular structural relaxation in electrical-transport properties of organic charge-transfer salts was recognized more than a decade ago.[25-38] Consideration of both the electronic and the intramolecular structural localization conditions is essential in understanding the properties of organic conducting salts. Electron localization is present in TTF·TCNQ, since it shows a $4k_f$ CDW in addition to a $2k_f$ CDW.[4e,7] A number of experimental studies on TTF·TCNQ suggest that the $2k_f$ and $4k_f$ CDW's originate primarily from the $TCNQ^{0.59-}$ and $TTF^{0.59+}$ stacks, respectively.[4e,7e-h,11] Thus, according to the explanation based upon electronic localization,[12] electrons in the $TTF^{0.59+}$ stacks are localized (i.e., $U/4|\beta| > 1$) while those in the TCNQ stacks are delocalized (i.e., $U/4|\beta| < 1$). This explanation, though consistent with the observation that electrons in the $TCNQ^{0.59-}$ stacks are the dominant carriers of the electrical conductivity in TTF·TCNQ,[13] leads to a number of difficulties.[4e,11,14] For instance, a difference of $U/4|\beta|$ between the $TTF^{0.59+}$ and the $TCNQ^{0.59-}$ stacks is expected to lead to a difference of electron-spin susceptibility between the two stacks, contrary to experimental observations.[4e,14,15] Furthermore, X-ray scattering studies suggest that a $2k_f$ CDW may also have to be present in the $TTF^{0.59+}$ stacks,[16] which is difficult to explain if $U/4|\beta| > 1$ for the $TTF^{0.59+}$ stacks.[4e] In fact, ^1H and ^{13}C NMR studies on TTF·TCNQ lead to the estimates of $U/4|\beta|$ less than unity for the $TTF^{0.59+}$ and the $TCNQ^{0.59-}$ stacks (0.75 and 0.81, respectively).[11,15a,17] These $U/4|\beta|$ values, though derived by using the formulas valid for small-U limit (i.e., $U/4|\beta| < 1$), do not vary significantly between small-U and large-U limits.[11] Thus, if electronic localization does not occur in TTF·TCNQ as suggested by these $U/4|\beta|$ values, how can one account for the occurrence of a $4k_f$ CDW in the $TTF^{0.59+}$ stacks? In this work, we propose that intramolecular structural localization is responsible for the $4k_f$ CDW.

In the following, we will first derive a simple empirical expression for the intramolecular structural localization condition. Then we will exemplify how electronic and intramolecular structural localizations affect the electronic structures of a molecular stack. This will be achieved by discussing the band electronic structures calculated for the mono-valence and mixed-valence structures of $TTF^{1/2+}$ and $TTF^{2/3+}$ stacks. On the basis of this analysis, we will formulate simple structural models of $2k_f$ and $4k_f$ CDW's in terms of intramolecular and intermolecular distortions.

I. Localization Conditions

Electronic localization in a molecular stack is very similar to that in a molecular dimer (i.e., any two adjacent molecules of the stack).[2c,6] Thus, intramolecular structural localization in a molecular stack is expected to be in essence similar to that in a molecular dimer.[18] If a partially oxidized donor stack has a mixed-valence structure, any two adjacent molecules of the stack are either D^+D^+, D^+D^0, or D^0D^0. Therefore, factors affecting the electronic and intramolecular structural localizations of the stack may be examined by simply considering the molecular dimers D^+D^+ and D^+D^0. Our discussion is simplified by taking into account only the HOMO, χ, and its electrons for each donor molecule. This simplification is reasonable, since the highest

(16) (a) Schultz, T. D. *Solid State Commun.* **1977**, *22*, 289. (b) Bak, P.; Emery, V. J. *Phys. Rev. Lett.* **1976**, *36*, 978.
(17) Soda, G.; Jérome, D.; Weger, M.; Fabre, J. M.; Giral, L. *Solid State Commun.* **1976**, *18*, 1417.
(18) Shaik, S. S. *J. Am. Chem. Soc.* **1982**, *104*, 5328.
(19) (a) Phillips, T. E.; Kistenmacher, T. J.; Ferraris, J. P.; Cowan, D. O. *J. Chem. Soc., Chem. Commun.* **1973**, 471. (b) Kistenmacher, T. J.; Phillips, T. E.; Cowan, D. O. *Acta Crystallogr., Sect. B: Struct. Crystallogr. Cryst. Chem.* **1974**, *B30*, 763. (c) Schultz, A. J.; Stucky, G. D.; Blessing, R. H.; Coppens, P. *J. Am. Chem. Soc.* **1976**, *98*, 3194.
(20) (a) Etemad, S.; Penny, T.; Engler, E. M.; Scott, B. A.; Seiden, P. *Phys. Rev. Lett.* **1975**, *34*, 741. (b) Etemad, S.; Engler, E. M.; Schultz, T. D.; Penny, T.; Scott, B. A. *Phys. Rev. B: Condens. Matter* **1978**, *17*, 513.
(21) The bandwidth of the donor stack is calculated to be $4|\beta| = 0.47$ eV for TTF·TCNQ and $4|\beta| = 0.59$ eV for TSF·TCNQ. See: Herman, F. *Phys. Scr.* **1977**, *16*, 303.
(22) (a) Whangbo, M.-H.; Hoffmann, R.; Woodward, R. B. *Proc. R. Soc. London, A* **1979**, *366*, 23. Whangbo, M.-H.; Hoffmann, R. *J. Am. Chem. Soc.* **1978**, *100*, 6093.
(23) (a) Hoffmann, R. *J. Chem. Phys.* **1963**, *39*, 1397. (b) The exponent ζ_μ and the valence shell ionization potential $H_{\mu\mu}$ (eV) for the Slater type orbital χ_μ employed in the present work are as follows: 1.625, −21.4 for C 2s; 1.625, −11.4 for C 2p; 1.817, −20.0 for S 3s; 1.817, −13.3 for S 3p; 1.3, −13.6 for H 1s.
(24) (a) Cooper, W. F.; Kenney, N. C.; Edmonds, J. W.; Nagel, A.; Wudl, F.; Coppens, P. *Chem. Commun.* **1971**, 889. (b) Kistenmacher, T. J.; Rossi, M.; Chiang, C. C.; Van Duyne, R. P.; Cape, T.; Siedle, A. R. *J. Am. Chem. Soc.* **1978**, *100*, 1958. (c) Yakushi, K.; Nishimura, S.; Sugano, T.; Kuroda, H.; Ikemoto, I. *Acta Crystallogr., Sect. B: Struct. Crystallogr. Cryst. Chem.* **1980**, *B36*, 358.
(25) Haddon, R. C. *Aust. J. Chem.*, **1975**, *28*, 2333.
(26) (a) Kistenmacher, T. J.; Emge, T. J.; Shu, P.; Cowan, D. O. *Acta Crystallogr., Sect. B: Struct. Crystallogr. Cryst. Chem.* **1979**, *B35*, 772. (b) Anderson, J. R.; Bechgaard, K.; Jacobsen, C. S.; Rindorf, G.; Soling, H.; Thorp, N. *Acta Crystallogr., Sect. B: Struct. Crystallogr. Cryst. Chem.* **1978**, *B34*, 1901. (c) Bechgaard, K.; Kistenmacher, T. J.; Bloch, A. N.; Cowan, D. O. *Acta Crystallogr., Sect. B: Struct. Crystallogr. Cryst. Chem.* **1977**, *B33*, 417.
(27) (a) Wudl, F. *J. Am. Chem. Soc.* **1975**, *97*, 1962. (b) Wudl, F.; Kaplan, M. L. *Inorg. Synth.* **1979**, *19*, 27.
(28) (a) Huizinga, S.; Kommandeur, J.; Swatzky, G. A.; Thole, B. T.; Kopina, K.; de Jonge, W. J. M.; Roos, J. *Phys. Rev. B: Condens. Matter* **1979**, *19*, 4723. (b) Huizinga, S.; Kommandeur, J.; Sawatzky, G. A.; Kopinga, K.; de Jonge, W. J. M. *Lect. Notes Phys.* **1979**, *96*, 45. (c) Sawatzky, G. A.; Huizinga, S.; Kommandeur, J. In "Quasi One-Dimensional Conductors II"; Ehlers, J., Hepp, K., Kippenhahn, R., Weidenmuller, H. A., Zittartz, J., Eds.; Springer-Verlag: Berlin, 1979; p 34.
(29) Two molecular species of each $(TNCQ)_2^-$ dimeric unit are somewhat different due presumably to countercations. See: (a) Bozio, R.; Pecile, C.; Tosi, P. *J. Phys. (Les Ulis, Fr.)* **1983**, *44* (C3), 1453. (b) Bosch, A.; van Bodegom, B. *Acta Crystallogr., Sect. B: Struct. Crystallogr. Cryst. Chem.* **1977**, *B33*, 3013.
(30) Calculations[21,31] without sulfur 3d orbitals show that the bandwidth of the $TTF^{0.59+}$ stack is somewhat smaller than that of the $TCNQ^{0.59-}$ stack. For example, $4|\beta| = 0.120$ and 0.145 eV for the $TTF^{0.59+}$ and the $TCNQ^{0.59-}$ stacks, respectively.[31b] Our qualitative conclusions based upon the intramolecular structural localization condition, eq 8, are not affected at all even if such calculated bandwidths are employed in our analysis.
(31) (a) Berlinsky, A. J.; Carolan, J. F.; Weiler, L. *Solid State Commun.* **1974**, *15*, 795. (b) Herman, F.; Salahub, D. L.; Messmer, R. P. *Phys. Rev. B: Solid State* **1977**, *16*, 2453.
(32) Weyl, C.; Engler, E. M.; Bechgaard, K.; Jehanno, G.; Etmad, S. *Solid State Commun.* **1976**, *19*, 925.
(33) Beni, G.; Pincus, P.; Kanamori, J. *Phys. Rev. B: Solid State* **1974**, *10*, 1896.
(34) Bechgaard, K.; Carneiro, K.; Rasmussen, F. B.; Olsen, M.; Rindorf, G.; Jacobsen, C. S.; Pedersen, H. J.; Scott, J. C. *J. Am. Chem. Soc.* **1981**, *103*, 2440.
(35) (a) Yagubskii, E. B.; Shchegolev, I. F.; Laukhin, V. N.; Kononovich, P. A.; Karatsovnik, M. W.; Zvarykina, A. V.; Buravov, L. I. *JETP Lett. (Engl. Transl.)* **1984**, *39*, 12. (b) Crabtree, G. W.; Carlson, K. D.; Hall, L. N.; Copps, P. T.; Wang, H. H.; Emge, T. J.; Beno, M. A.; Williams, J. M. *Phys. Rev. B: Condens. Matter* **1984**, *30*, 2958. (c) Williams, J. M.; Emge, T. J.; Wang, H. H.; Beno, M. A.; Copp, P. T.; Hall, L. N.; Carlson, K. D.; Crabtree, G. W. *Inorg. Chem.* **1984**, *23*, 2558. (d) Williams, J. M.; Wang, H. H.; Beno, M. A.; Emge, T. J.; Sowa, L. M.; Copps, P. T.; Behroozi, F.; Hall, L. N.; Carlson, K. D.; Crabtree, G. W. *Inorg. Chem.* **1984**, *23*, 3839.
(36) Sato, N.; Saito, G.; Inokuchi, H. *Chem. Phys.* **1983**, *76*, 79.
(37) Jacobsen, C. S.; Tanner, D. B.; Bechgaard, K. *Mol. Cryst. Liq. Cryst.* **1982**, *79*, 25.
(38) (a) Chaiken, P. M.; Garito, A. F.; Heeger, A. J. *J. Chem. Phys.* **1973**, *58*, 2336. (b) Horovitz, B.; Weger, M.; Gutfreund, H. *Phys. Rev. B: Solid State* **1974**, *9*, 1246. (c) Epstein, A. J.; Conwell, E. M.; Sandman, D. J.; Miller, J. S. *Solid State Commun.* **1977**, *23*, 355.

occupied band of a molecular stack is mainly derived from the HOMO of each molecule.

I.A. Electronic Localization in D^+D^+. An electron-localized state of D^+D^+, in which an unpaired electron resides on each D^+, may be represented by **4a**.[6] An electron-delocalized state **4b** has

4a 4b

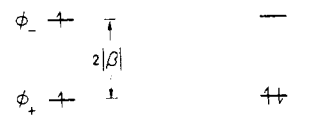

5a 5b

two electrons equally shared between two D^+ species. Within the framework of molecular orbital (MO) theory, **4a** and **4b** are described by the electronic states **5a** and **5b**, respectively, where ϕ_+ and ϕ_- are the bonding and antibonding combinations of the HOMO's χ_a and χ_b of $D_a^+D_b^+$, respectively.

$$\phi_+ = (\chi_a + \chi_b)/2^{1/2} \qquad \phi_- = (\chi_a - \chi_b)/2^{1/2} \tag{1}$$

The ϕ_+ and ϕ_- levels are separated in energy by $2|\beta|$, where $\beta = \langle\chi_a|H|\chi_b\rangle$. The relative stability of **5a** and **5b**, and hence that of **4a** and **4b**, is governed by the balance between the resonance integral and on-site repulsion:[6]

$$\Delta E(D^+D^+) \equiv E(\mathbf{5a}) - E(\mathbf{5b}) = 2|\beta| - U/2 \tag{2}$$

Thus when $U > 4|\beta|$, the localized state is more stable than the delocalized state. Either in **4a** or in **4b** the two D^+ species are *identical*; i.e., **4a** and **4b** have a *mono-valence structure*. However, the structure of D^+ in **4a** would be somewhat different from that in **4b**, as the electronic structures **5a** and **5b** are not identical. The electron localization **4b** → **4a** might then induce some intramolecular geometry relaxation in both D^+'s. Be it as it may, the electronic localization does not change the mono-valence nature of D^+D^+.

I.B. Intramolecular Structural Localization in D^+D^0. As shown in **6**, the mixed-valence structure of D^+D^0 can be either $D_a^+D_b^0$ or $D_a^0D_b^+$. The mono-valence structure $(DD)^+$, shown in **7a**, has

6a 6b

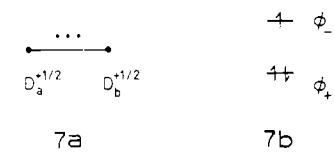

7a 7b

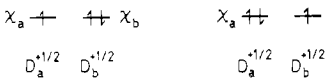

8a 8b

all three electrons equally shared by the two donor species $D^{1/2+}$. The electronic structure of **7a** can be described by **7b** within the framework of MO theory. Then it is easy to show that the total on-site repulsion associated with **7a** is U, just as in **6a** or **6b**. Therefore, *on-site repulsion is not a factor governing the relative stability of the mixed-valence and mono-valence structures of D^+D^0.*

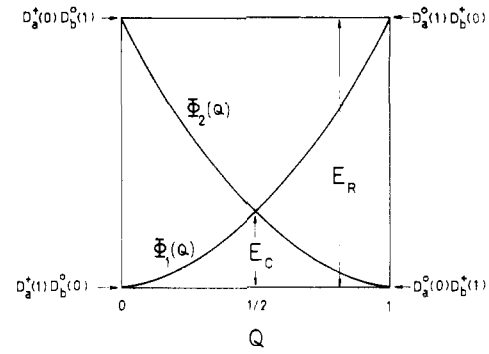

Figure 1. Correlation diagram for the ground and excited configurations of $D_a^+D_b^0$ and $D_a^0D_b^+$.

Let us examine the energetic factors associated with the structural localization **7a** → **6**. To specify the relaxed and nonrelaxed geometries of D^+ and D^0, it is convenient to employ the notation $D_i^{q+}(p)$ to denote the donor i (i = a, b) having the geometry optimum for D^{q+} but with an actual charge $p+$. The D^+ and D^0 species are most stable when they adopt their optimum geometries, so that the ground configurations of $D_a^+D_b^0$ and $D_a^0D_b^+$ are $D_a^+(1)D_b^0(0)$ and $D_a^0(0)D_b^+(1)$, respectively. These configurations are interchanged upon electron transfer from D^0 to D^+. Suppose that this electron transfer occurs without relaxing the geometries of the $D^+(1)$ and $D^0(0)$ species involved. Then the resulting electron-transferred configurations $D_a^+(0)D_b^0(1)$ and $D_a^0(1)D_b^+(0)$ are less stable than the ground configurations and, hence, are the "excited" configurations of $D_a^+(1)D_b^0(0)$ and $D_a^0(0)D_b^+(1)$, respectively. The energy difference between the excited and the ground configurations of D^+D^0, which will be referred to as the intramolecular relaxation energy E_R, is equal to the magnitude of energy lowering that results when the geometry of the excited configuration is relaxed to that of the ground configuration.

In discussing the relative stabilities of mono- and mixed-valence structures, it is easy to run into a misconception such as follows: Since the electronic configurations D^+D^0 and D^0D^+ are energetically equivalent, their linear combinations $D^+D^0 \pm D^0D^+$ may be regarded as valid. Thus, one may suppose these combinations give rise to a mono-valence structure $D^{1/2+}D^{1/2+}$, thereby reaching the conclusion that no mixed-valence structure occurs. This reasoning is erroneous on the basis of both experiment and theory. The occurrence of mixed-valence structures is an experimental fact, even for the $TTF^{0.59+}$ stacks of TTF·TCNQ[10a] that apparently look mono-valent under the time scale of single-crystal X-ray studies.[19] In addition, a variational solution of quantum mechanics shows that a symmetry-adapted state (e.g., mono-valence and metallic states) is not necessarily more stable than its alternative, a symmetry-broken state (e.g., mixed-valence and antiferromagnetic states).[39] Construction of new electronic states by linearly combining a number of electronic configurations is valid only when all the configurations refer to an identical set of molecular geometries involved. The molecular species $D_a^+(1)$ and $D_a^0(0)$ have different geometries, and so do $D_b^+(1)$ and $D_b^0(0)$. Therefore, linear combinations of the configurations $D_a^+(1)D_b^0(0)$ and $D_a^0(0)D_b^+(1)$ are meaningless although these configurations are energetically equivalent. However, meaningful new states are obtained by linear combinations of $D_a^+(1)D_b^0(0)$ and $D_a^+(0)D_b^0(1)$ [or $D_a^0(0)D_b^+(1)$ and $D_a^0(1)D_b^+(0)$]. However, these configurations have different energies and hence would have different

(39) (a) Löwdin, P.-O. *Rev. Mod. Phys.* **1963**, *35*, 496. (b) Löwdin, P.-O. *Adv. Chem. Phys.* **1969**, *14*, 283. (c) Thouless, D. J. "The Quantum Mechanics of Many Body Systems"; Academic: New York, 1961. (d) Cizek, J.; Paldus, J. *J. Chem. Phys.* **1967**, *47*, 3976.

weights in the new states.[40] Consequently, a mixed-valence character would remain for the linearly combined states.

Figure 1 shows how the ground and excited configurations of $D_a^+D_b^0$ are related to those of $D_a^0D_b^+$ as a function of the reaction coordinate Q ($0 \leq Q \leq 1$) that converts $D_a^+D_b^0$ to $D_a^0D_b^+$. As Q changes from 0 to 1, the ground configuration $D_a^+(1)D_b^0(0)$ is gradually converted to the excited configuration $D_a^0(1)D_b^+(0)$ along the curve $\Phi_1(Q)$. Likewise, the excited configuration $D_a^+(0)D_b^0(1)$ gradually becomes the ground configuration $D_a^0(0)D_b^+(1)$ along the curve $\Phi_2(Q)$. The two correlation curves cross at the midpoint $Q = {}^1/_2$, where the two donor species have an identical geometry (i.e., that of $D^{1/2+}$). The crossing point lies at E_C above the energy of the ground configuration.

At any point of Q in Figure 1, the ground and excited states of D^+D^0 ($\Psi_1(Q)$ and $\Psi_2(Q)$, respectively) are expressed as a linear combination of $\Phi_1(Q)$ and $\Phi_2(Q)$. For an ideal mixed-valence structure of D^+D^0 the ground and excited states at $Q = 0$ are approximated by

$$\Psi_1(0) \simeq \Phi_1(0) = D_a^+(1)D_b^0(0)$$
$$\Psi_2(0) \simeq \Phi_2(0) = D_a^+(0)D_b^0(1) \tag{3}$$

Thus the energy difference between $\Psi_1(0)$ and $\Psi_2(0)$ is equal to E_R, which can be estimated as follows:

$$\begin{aligned} E_R &= E[D_a^+(0)D_b^0(1)] - E[D_a^+(1)D_b^0(0)] \\ &= \{E[D_b^0(1)] - E[D_a^+(1)]\} + \{E[D_a^+(0)] - E[D_b^0(0)]\} \\ &= (IP^v - IP^a) + \{E[D_a^+(0)] - E[D_b^0(0)]\} \end{aligned} \tag{4a}$$

where IP^v and IP^a are the vertial and adiabatic ionization potentials of D, respectively. The last term of eq 4a is approximately the same as $(IP^v - IP^a)$, so that

$$E_R \simeq 2(IP^v - IP^a) \tag{4b}$$

At the crossing point $Q = {}^1/_2$, the ground and the excited states are expressed by[18]

$$\Psi_1({}^1/_2) = [\Phi_1({}^1/_2) - \Phi_2({}^1/_2)]/2^{1/2}$$
$$\Psi_2({}^1/_2) = [\Phi_1({}^1/_2) + \Phi_2({}^1/_2)]/2^{1/2} \tag{5}$$

where

$$\Phi_1({}^1/_2) = D_a^{1/2+}(1)D_b^{1/2+}(0)$$
$$\Phi_2({}^1/_2) = D_a^{1/2+}(0)D_b^{1/2+}(1) \tag{6}$$

Since the two donor species are idential in structure, $\Psi_1({}^1/_2)$ and $\Psi_2({}^1/_2)$ are the ground and the excited states of the mono-valence structures **7a**, respectively. In terms of molecular orbitals, $\Phi_1({}^1/_2)$ and $\Phi_2({}^1/_2)$ are represented by **8a** and **8b**, respectively, which differ by an electron transfer from χ_a to χ_b. The interaction energy between $\Phi_1({}^1/_2)$ and $\Phi_2({}^1/_2)$ is related to the resonance integral β between the HOMO's χ_a and χ_b as follows:[18]

$$\langle\Phi_1({}^1/_2)|H|\Phi_2({}^1/_2)\rangle = -\langle\chi_a|H|\chi_b\rangle = -\beta \tag{7}$$

Consequently, the energies of $\Psi_1({}^1/_2)$ and $\Psi_2({}^1/_2)$ are lowered and raised by $|\beta|$ with respect to the energy of the crossing point. In the ground state of D^+D^0, therefore, the stability of the mixed-valence structure relative to that of the mono-valence structure is given by

$$\begin{aligned} \Delta E(D^+D^0) &\equiv E(\mathbf{6a}) - E(\mathbf{7a}) \\ &= |\beta| - E_C \end{aligned} \tag{8}$$

Figure 2a shows the potential energy surfaces of $\Psi_1(Q)$ and $\Psi_2(Q)$ relevant for a case when the mixed-valence structure is more stable (i.e., $E_C > |\beta|$), and Figure 2b those relevant for a case when the mono-valence structure is more stable (i.e., $E_C < |\beta|$). If the mono-valence structure is more stable, the $|\Delta E(D^+D^0)|$ value of eq 8 becomes the energy barrier for the electron-hopping transition **6a** → **6b**.

(40) Albright, T. A.; Burdett, J. K.; Whangbo, M.-H. "Orbital Interactions in Chemistry"; Wiley: New York, 1985.

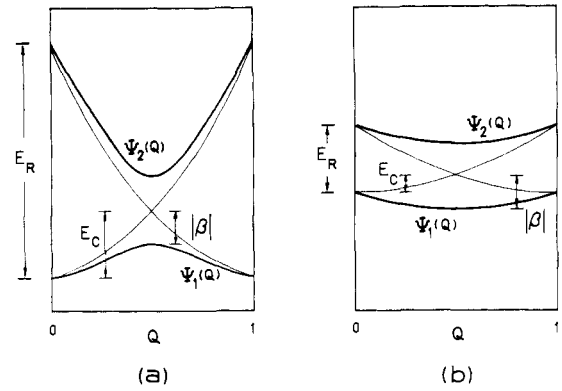

Figure 2. Correlation diagram for the ground and excited states of $D_a^+D_b^0$ and $D_a^0D_b^+$: (a) $E_C > |\beta|$; (b) $E_C < |\beta|$.

A similar analysis exists for a partially reduced acceptor stack (A^-A^0). Here the intramolecular relaxation energy is related to the corresponding difference between the vertical and the adiabatic electron affinities (EA) such that

$$E_R \simeq 2(EA^v - EA^a) \tag{9}$$

and $\Delta E(A^-A^0) = |\beta| - E_C$ as in eq 8. Thus, in contrast to electronic localization, intramolecular structural localization not only creates unpaired electrons but also changes the geometry of a stack from a mono-valence to a mixed-valence structure.

I.C. Applications. Just as the electronic localization condition derived for D^+D^+ (eq 2) can be used to discuss electron localization in donor stacks, the intramolecular structural localization condition derived for D^+D^0 and A^-A^0 (eq 8 and Figure 2) may be employed to describe intramolecular structural localization in donor or acceptor stacks. The intramolecular structural localization condition is valid for those cases when both mixed-valence and mono-valence structures have the same extent of on-site repulsion (see section I.B). In principle, therefore, the intramolecular structural localization condition is concerned with the question of whether an electron-localized state leads to a mixed-valence or a mono-valence structure, but the electronic localization condition is concerned with that of whether a mono-valence structure adopts an electron-localized or an electron-delocalized state (e.g., **4a** vs. **4b**). However, it should be noted that any factor favoring a mixed-valence structure will enhance the stability of an electron-localized state, since such a factor leads to electron localization as does electron–electron repulsion.

It is clear from Figure 1 that the value of E_C will increase with that of E_R. Thus, the balance between intramolecular relaxation (E_R) and intermolecular resonance interaction (β) determines whether or not the mixed-valence structure is more stable than the mono-valence structure in D^+D^0 and in A^-A^0. Let us now estimate the values of $\Delta E(D^+D^0)$ and $\Delta E(A^-A^0)$ (eq 8) in terms of some experimental quantities associated with the donor D and the acceptor A. The value of E_C can be expressed in terms of E_R, once a functional form of $\Phi_i(Q)$ (i = 1, 2) is specified. It is reasonable to assume that $\Phi_i(Q)$ is a quadratic function of Q;[18] i.e.

$$\Phi_1(Q) \simeq E_R Q^2 \qquad \Phi_2(Q) \simeq E_R(1 - Q)^2 \tag{10}$$

which leads to the result $E_C \simeq E_R/4$, so that

$$\Delta E(D^+D^0) \simeq |\beta| - E_R/4 \qquad \Delta E(A^-A^0) \simeq |\beta| - E_R/4 \tag{11}$$

Namely, the mixed-valence structure **6a** or **6b** is more stable than the mono-valence structure **7a** when $E_R > 4|\beta|$. And a similar relationship exists for the analogous acceptor stack.

Table I lists the $E_R/4$ values of some donor molecules estimated in terms of eq 4b. From the definition of E_R, it is obvious that a large value of E_R means a strong tendency for intramolecular relaxation and hence for a mixed-valence structure. Table I shows that E_R is large for TTF but considerably small for TTF derivatives and that E_R is small for TSF and TSF derivatives. It is noted that E_R value of TTF estimated from the semiempirical SCF–MO

Table I. $E_R/4$ Values of Donor Molecules Estimated from Their IP^v and IP^a Values [a,b]

molecule	$E_R/4$	molecule	$E_R/4$
TTF	0.26	TSF	0.11
TMTTF	0.17	TMTSF	0.16
HMTTF	0.18	HMTSF	0.11
BEDT-TTF	0.15		

[a] $E_R/4 = (IP^v - IP^a)/2$, where the values of IP^v and IP^a were taken from ref 36. [b] All values are in electronvolts.

Table II. $E_R/4$, $|\beta|$, and ΔE Values Estimated for Molecular Stacks[a,b]

salt	stack	$E_R/4$	$\|\beta\|$	ΔE
TTF·TCNQ	$TTF^{0.59+}$	0.26	0.16[c]	−0.10
TSF·TCNQ	$TSF^{0.63+}$	0.11	(>0.16)	(>0.05)
$(TMTSF)_2PF_6$	$TMTSF^{1/2+}$	0.16	0.25[d]	0.09
TTF·TCNQ	$TCNQ^{0.59-}$	(<0.10)	0.10[c]	(>0.0)

[a] ΔE refers to $\Delta E(D^+D^0)$ for a donor stack but $\Delta E(A^-A^0)$ for an acceptor stack. [b] All values are in electronvolts. [c] Reference 11. [d] Reference 37.

calculations[25] carried out on TTF^0 and TTF^+ is quite small, in disagreement with the experimental estimate given in Table I.

Given the experimentally estimated bandwidth W for an organic conducting salt, the $|\beta|$ value of its molecular stack may be approximated by $W/4$. Use of such a $|\beta|$ value, together with the $E_R/4$ value of the stacking molecule in eq 11, leads to a qualitative estimate for $\Delta E(D^+D^0)$ and $\Delta E(A^-A^0)$. Summarized in Table II are the $E_R/4$, $|\beta|$, and ΔE values estimated for the $TTF^{0.59+}$, $TSF^{0.63+}$, $TMTSF^{0.5+}$, and $TCNQ^{0.59-}$ stacks present in the most extensively studied compounds TTF·TCNQ, TSF·TCNQ, and $(TMTSF)_2PF_6$. An experimental estimate for the bandwidth W of the $TSF^{0.63+}$ stack is not available. However, TSF·TCNQ is very similar to TTF·TCNQ in structure,[19,20] and selenium 4p orbitals lead to better intermolecular overlap than sulfur 3p orbitals. Thus, the $|\beta|$ value of the $TSF^{0.63+}$ stack in TSF·TCNQ is expected to be greater than that of the $TTF^{0.59+}$ stacks in TTF·TCNQ.[21] From Table II, the following are observed: The $TTF^{0.59+}$ stacks of TTF·TCNQ prefer a mixed-valence structure, while the $TSF^{0.63+}$ stacks of TSF·TCNQ and the $TMTSF^{0.5+}$ stacks of $(TMTSF)_2PF_6$ prefer a mono-valence structure. The primary cause for this difference is that the tendency for intramolecular relaxation is significantly greater for TTF than for TSF and TMTSF.

According to XPS studies,[10] the $TTF^{0.59+}$ stacks of TTF·TCNQ adopt a mixed-valence structure while the $TMTSF^{0.5+}$ stacks of $(TMTSF)_2X$ ($X^- = PF_6^-$, AsF_6^-, ClO_4^-, IO_4^-, BF_4^-) have a mono-valence structure. Thus, the predictions based upon the structural localization condition of eq 11 are consistent with the results of the XPS studies. According to the energy factors governing the electronic and the intramolecular structural localization conditions, a given molecular stack may belong to one of the four different cases I–IV summarized in Table III. It is clear that the occurrence of either a mono- or a mixed-valence structure alone cannot reveal whether the electrons in such a structure are localized or delocalized in the sense of the electronic localization condition ($4|\beta| < U$), which refers to the relative stability of the high-spin state with respect to that of the low-spin state in a mono-valence stack (e.g., **3a** vs. **3b**). It is also important to observe from Table III that the occurrence of high-spin states in molecular stacks, and hence $4k_f$ CDW's (for details, see the next section), does not necessarily mean $U > 4|\beta|$. High-spin states may occur simply because $E_R > 4|\beta|$ even if $U < 4|\beta|$. Listed in the last column of Table III are some examples considered to represent cases II–IV (for details, see the next section).

Table II reveals that the stability of a mono-valence structure over a mixed-valence one is very slight. It is only when the E_R term becomes negligible that a mono-valence structure is expected to have appreciable stability over a mixed-valence one. In most common cases, which are represented in Tables I and II, E_R is not negligible. Consequently, an extrinsic factor such as counterions might play an important role in tipping the stability balance between mono-valence and mixed-valence structures.

Table III. Structural and Physical Properties Expected for the Four Different Situations Created by the Electronic and the Intramolecular Structural Localization Conditions

case	energy factor	observation	example
I	$E_R > 4\|\beta\|$ $U > 4\|\beta\|$	mixed-valence, high-spin, $4k_f$ CDW	
II	$E_R > 4\|\beta\|$ $U < 4\|\beta\|$	mixed-valence high-spin, $4k_f$ CDW	$TTF^{0.59+}$ stacks of TTF·TCNQ
III	$E_R < 4\|\beta\|$ $U > 4\|\beta\|$	mono-valence, high-spin, $4k_f$ CDW	$TCNQ^{0.5-}$ stacks of MEM·2TCNQ (19–335 K)
IV	$E_R < 4\|\beta\|$ $U < 4\|\beta\|$	mono-valence, low-spin, $2k_f$ CDW	$TCNQ^{0.59-}$ stacks of TTF·TCNQ

II. Structural Models of $2k_f$ and $4k_f$ Distortions

Let us now draw a link between the various localization mechanisms and the observed structural distortions. Any distortion of a molecular stack may be composed of intramolecular relaxation and/or intermolecular displacive distortion. To understand the nature of $2k_f$ and $4k_f$ CDW's on a molecular level, it is necessary to discuss these distortions from the viewpoint of intramolecular and intermolecular mechanisms. Toward this end, we carry out tight-binding-band calculations[22] (based upon the extended Hückel method[23]) for a few mono-valence and mixed-valence structures of $TTF^{0.5+}$ and $TTF^{2/3+}$ stacks. On the basis of these calculations and the structural and electron localization conditions, we formulate simple structural models of $2k_f$ and $4k_f$ CDW's.

II.A. Intramolecular Relaxation and the HOMO Character. Since the highest occupied bands of a partially oxidized TTF stack is largely derived from the HOMO of each TTF, it is important to see how the HOMO of $TTF^{\rho+}$ varies as a function of the fractional charge ρ. Shown in **9a** and **9b** are the C–C and C–S

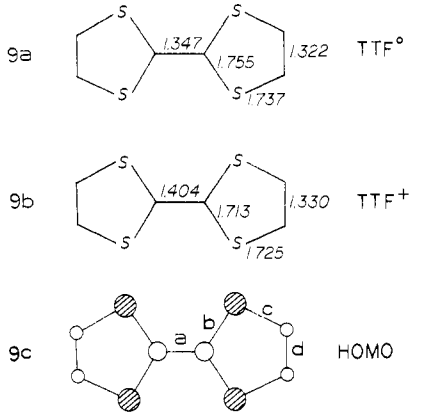

bond lengths of TTF^0 and TTF^+, respectively.[8,24] The bond length differences between the two species can be easily explained in terms of the HOMO nodal properties[25] shown in **9c**. The HOMO is bonding for bonds a and d but antibonding for bonds b and c. Therefore, electron removal from the HOMO of TTF^0 will weaken bonds a and d but strengthen bonds b and c. Consequently, TTF^+ possesses longer a and d bonds but shorter b and c bonds than does TTF^0. Such a structural difference between TTF^0 and TTF^+ is a primary cause for the relaxation energy E_R.

As far as the HOMO level is concerned, lengthening bonds a and d makes the HOMO level less bonding while shortening bonds b and c makes the HOMO more antibonding. Consequently, the HOMO level of $TTF^{\rho+}$ ($0 \le \rho \le 1$) is expected to increase as ρ changes from 0 to 1. For simplicity, the bond lengths and bond angles of $TTF^{\rho+}$ may be assumed to change as a linear function of ρ between the two extreme values given by TTF^0 and TTF^+. The HOMO level of thus obtained $TTF^{\rho+}$ is calculated to vary as a function of ρ, as shown in Figure 3. This general behavior is seen to be in agreement with the prediction based upon the HOMO nodal properties.

The HOMO nodal properties of TSF are similar to those of TTF shown in **9c** except that the atomic orbital weights are more

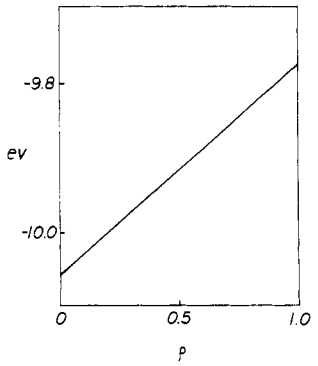

Figure 3. Energy of the HOMO of $TTF^{\rho+}$ as a function of ρ.

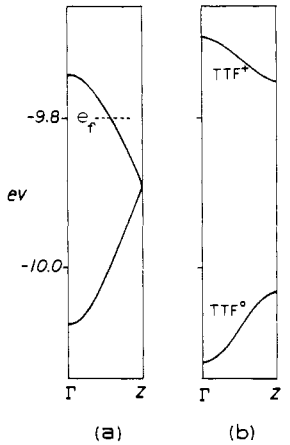

Figure 4. Bands of **10a** and **10b** derived from the HOMO of each donor species: (a) **10a**; (b) **10b**. Γ and Z refer to the Brillouin zone center and edge, respectively.

concentrated on the selenium atoms in TSF compared with those on the sulfur atoms in TTF. In addition, bonds b and c are longer in TSF than those in TTF. Thus, the HOMO of TSF is more nonbonding than that of TTF, so that the structural difference between TSF^0 and TSF^+ is not predicted to be as large as that between TTF^0 and TTF^+. In fact, the crystal structures of $TMTSF^0$ and $TMTSF^{\rho+}$ show that the bond length differences between $TMTSF^0$ and $TMTSF^{\rho+}$ ($\rho \neq 0$) are small.[26] Therefore, the aforementioned weaker tendency for intramolecular relaxation in TSF is related to the more nonbonding character of its HOMO relative to that of TTF.

II.B. Band Structures of $TTF^{1/2+}$ and $TTF^{2/3+}$ Stacks. Shown in **10a** and **10b** are the mono-valence and mixed-valence structures of a $TTF^{1/2+}$ stack, respectively. For the values of the inter-

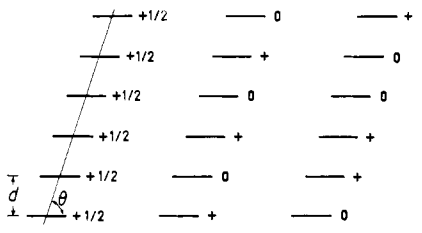

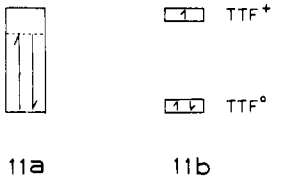

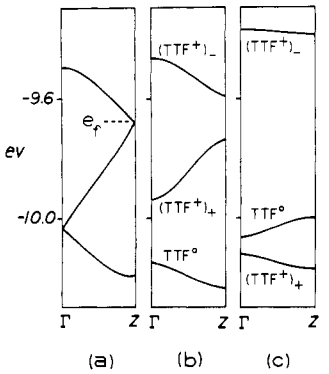

Figure 5. Bands of **12a–c** derived from the HOMO of each donor species: (a) **12a**; (b) **12b**; (c) **12c**. Γ and Z refer to the Brillouin zone center and edge, respectively.

molecular spacing d and the tilt angle θ taken from TTF·TCNQ,[19c] the band electronic structures of **10a** and **10b** are given by Figure 4, a and b, respectively. The doubly folded band of Figure 4a simply arises from the fact that $(TTF^{1/2+})_2$ was chosen as a unit cell for **10a**. If the mono-valence structure adopts a metallic state, the band is $^3/_4$-filled, as depicted in **11a**. The intramolecular relaxation **10a** → **10b** leads to the two split bands of Figure 4b, where the upper and lower subbands are largely the HOMO's of TTF^+ and TTF^0 in character, respectively. These band compositions result from the fact that the HOMO of TTF^+ is higher in energy than that of TTF^0 (see Figure 3). The two subbands of **10b** are quite flat, so they are likely to adopt a magnetic insulating state, **11b**, in which an odd electron is localized on each TTF^+ site. Then the electronic state change **11a** → **11b** is a metal–magnetic insulator transition, which is accompanied by the intramolecular relaxation **10a** → **10b**.

Shown in **12a–12c** are three structures of a $TTF^{2/3+}$ stack. It is the mixed-valence structure **12c** that is found in $(TTF)_3(BF_4)_2$.[8]

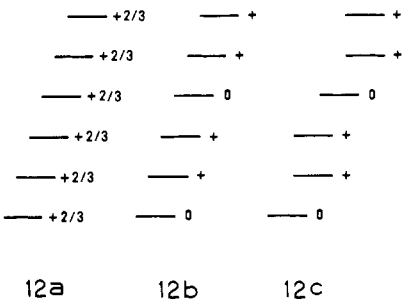

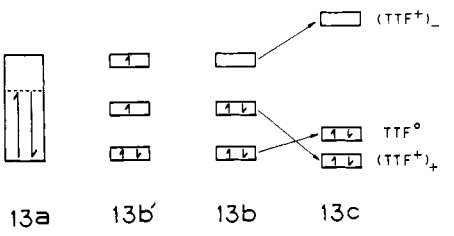

In **12c** each TTF^0·TTF^+·TTF^+ triad contains an eclipsing (ring-over-ring) arrangement of two TTF^+ species, while TTF^0 is slipped off to maintain a ring-over-central bond arrangement with $(TTF^+)_2$. The mono-valence structure **12a** may be imagined to lead to the observed structure **12c** by the intramolecular relaxation **12a** → **12b** followed by the intermolecular displacive distortion **12b** → **12c**.

The band structures of **12a–c** are shown in Figure 5, parts a–c, respectively. The triply folded band structure of Figure 5a is due to the fact that the unit cell of **12a** was chosen to be $(TTF^{2/3+})_3$. The metallic state of **12a** has the band $^2/_3$-filled as shown in **13a**. Upon the intramolecular distortion **12a** → **12b**, the unit cell size is tripled, and the band splits into three subbands. In Figure 5b,

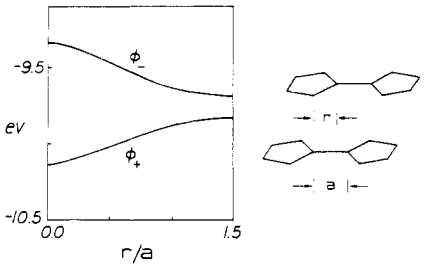

Figure 6. Energy splitting of the HOMO's of the two D^+ units as a function of the slipping parameter r/a.

the bottom subband has the HOMO character of TTF^0, and the top two subbands have that of TTF^+. The $(TTF^+)_+$ and $(TTF^+)_-$ subbands have the HOMO's of adjacent TTF^+ species combined in phase and out of phase, respectively. The electronic state of **12b** can be either nonmagnetic insulating as in **13b** or magnetic insulating as in **13b′**. In other words, an odd electron is localized on each TTF^+ site in **13b′**, while in 13b the "odd electrons" from each TTF^+ pair are equally shared between the two TTF^+ species. The "high-spin" state **13b′** becomes more stable than the "low-spin" state **13b**, when the energy gap between the $(TTF^+)_+$ and $(TTF^+)_-$ subbands is small.

Like **12b**, **12c** has a unit cell 3 times as large as that of **12a**, and its band consists of three subbands. However, upon the intermolecular displacive distortion **12b** → **12c**, the $(TTF^+)_+$ and $(TTF^+)_-$ subbands are lowered and raised in energy, respectively. Thus, in **12c** the $(TTF^+)_+$ subband is even lower in energy than the TTF^0 subband. This difference between **12b** and **12c** originates from the intermolecular interaction between adjacent TTF^+ species. Figure 6 shows how the extent of the HOMO–HOMO interaction in the dimer $(TTF^+)_2$ depends upon the slipping between the two TTF^+ species. When two TTF^+ species are eclipsed as in **12c**, the energy lowering of the $(TTF^+)_+$ subband that results from the intermolecular interaction is large enough to overcome the energy raising (induced by intramolecular relaxation) of the TTF^+ HOMO relative to the TTF^0 HOMO (Figure 3). Due to the large energy difference between the $(TTF^+)_+$ and $(TTF^+)_-$ subbands and that between the TTF^0 and $(TTF^+)_-$ subbands, the electronic state relevant for **12c** would be given by **13c**. This nonmagnetic insulating state is consistent with the fact that $(TTF)_3(BF_4)_2$ is an insulator.[27] Because of the strong intermolecular interaction between TTF^+ species, **13c** is expected to be more stable than either **13b** or **13b′**.

Both the **12a** → **12b** and the **12a** → **12c** distortions triple the unit cell size and open a band gap at the Fermi level of **12a**. Thus, the structural change **12a** → **12c** is a $2k_f$ distortion, and so is the intramolecular relaxation **12a** → **12b** if it is associated with the electronic state change **13a** → **13b**. Finally, it is noted that the intramolecular relaxation **12a** → **12b** is a metal–magnetic insulator transition when it is associated with the electronic state change **13a** → **13b′**.

II.C. $2k_f$ and $4k_f$ CDW's. The nature of the structural distortion that a molecular stack might undergo is intimately related to the electronic states involved, as we have seen in the previous sections. The concept of Peierls distortion does not allow us to predict what the distorted structure of a molecular stack would be really like on a molecular level. Therefore, in formulating simple structural models for $2k_f$ and $4k_f$ CDW's, it is necessary to consider both electronic and intramolecular structural localizations. Let us now return to the problem of the $TTF^{1/2+}$ stack **10**. The metallic state **11a** is $^3/_4$-filled so that the $2k_f$ CDW appropriate for this band filling is a tetramerization. Thus, the dimerization $(TTF^{1/2+})_\infty$ → $(TTF^0{\cdot}TTF^+)_\infty$, i.e., **10a** → **10b**, is a $4k_f$ CDW associated with the intramolecular structural localization **11a** → **11b**. An alternative mixed-valence structure, **10c**, has a unit cell 4 times as large as that of $(TTF^{1/2+})_\infty$. In **10c** every adjacent TTF^+ species might even pair up, if allowed structurally as in $(TTF)_3(BF_4)_2$, to give rise to a nonmagnetic insulating structure $[TTF^0{\cdot}TTF^0{\cdot}(TTF^+)_2]_\infty$. Then the structural change **10a** → **10c** would be a $2k_f$ CDW. The ground state of a $^1/_4$-empty molecular stack such as $(TTF^{0.5+})_\infty$ is found to be given by **10c** if the stack prefers a mixed-valence structure.[33]

To summarize, the $2k_f$ and $4k_f$ CDW's allowed for a $D^{1/2+}$ stack are primarily governed by intramolecular relaxation as illustrated in **14**, provided that this stack has a strong tendency for a mixed-valence structure $E_R > 4|\beta|$. On the other hand, if a $D^{1/2+}$ stack prefers a mono-valence structure ($E_R < 4|\beta|$), its $2k_f$ and $4k_f$ CDW's are mainly determined by intermolecular displacive distortion as shown in **15**. In contrast to the $4k_f$ structure of **14**, that of **15** has an odd electron equally shared between the two molecules of each dimeric unit. In general, the $2k_f$ and $4k_f$ CDW's of any donor or acceptor stack may be accounted for in terms of intramolecular and intermolecular distortions as in **14** and **15**. An important point to note is that electron localization is responsible for a $4k_f$ structure either in a mixed-valence or in a mono-valence structure.

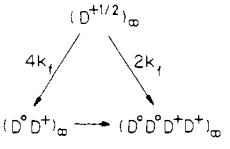

14

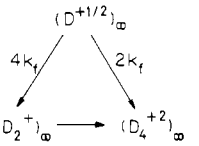

15

The models of $2k_f$ and $4k_f$ CDW's summarized in **14** and **15** are not complete in that they neither include the role of counterions X^- nor take into account interstack interactions. Nevertheless, those models present a convenient starting point of discussion in understanding various experimental observations of organic conducting salts on a molecular level. With this in mind, let us briefly review some pertinent experimental data. An example that roughly fits the model **15** is observed for the acceptor analogue MEM·2TCNQ (MEM^+ = methylethylmorpholinium cation),[4d,28] which consists of $TCNQ^{1/2-}$ stacks. Each $TCNQ^{1/2-}$ stack has a $^1/_4$-filled band derived from the LUMO of each TCNQ. At high temperature ($T > 335$ K), MEM·2TCNQ has uniform stacks $(TCNQ^{1/2-})_\infty$. As temperature is lowered (19 K $< T <$ 335 K), a $4k_f$ structure $[(TCNQ)_2^-]_\infty$ is observed. This dimerized stack has an odd electron shared between the two TCNQ molecules in each dimeric unit.[29] The temperature dependence of the magnetic susceptibility of the $4k_f$ structure shows an antiferromagnetic arrangement of spins. Thus, the structural change from the uniform to the $4k_f$ structure is a metal–magnetic insulator transition. Further lowering of temperature ($T < 19$ K) leads to a $2k_f$ structure in which the unit cell size is quadrupled with respect to that of the uniform structure.

As already noted, both $2k_f$ and $4k_f$ CDW's are present in TTF·TCNQ.[4,7] Three phase transitions occur in TTF·TCNQ at $T_1 = 54$ K, $T_2 = 49$ K, and $T_3 = 38$ K.[4,7] Magnetic susceptibility measurements[15b,c] and ^{13}C NMR studies[11] show that the T_1 transition involves the $TCNQ^{0.59-}$ stacks, while the T_2 and T_3 transitions involve the $TTF^{0.59+}$ stacks.[4e,6e-h,11] The observations that a $4k_f$ CDW is present in the $TTF^{0.59+}$ stacks,[4e,7e-h,11] that $U/4|\beta| < 1$ for the $TTF^{0.59+}$ stacks,[11,15a] that the electrons of the $TTF^{0.59+}$ stacks are not dominant carriers of the electrical conductivity in TTF·TCNQ,[13] and that the $TTF^{0.59+}$ stacks have a mixed-valence structure[10a] are all explained in terms of intramolecular structural localization (i.e., $E_R/4|\beta| > 1$) in the $TTF^{0.59+}$ stacks. The $4k_f$ and $2k_f$ CDW's in the $TTF^{0.59+}$ stacks may be rationalized by analogy with the $4k_f$ and $2k_f$ structures of a mixed-valence donor chain with a $^1/_4$-empty band (see **10b**, **10c** and **14**), respectively.

Concerning whether or not the $TCNQ^{0.59-}$ stacks of TTF·TCNQ have a mixed-valence structure, XPS studies[10a] are not conclusive since the nitrogen 1s peaks are complicated with shake-up satellites. However, the facts that a $4k_f$ CDW is absent in the $TCNQ^{0.59-}$ stacks and that electrons of the $TCNQ^{0.59-}$ stacks are dominant carriers of the electrical conductivity in TTF·TCNQ indicate that the $TCNQ^{0.59-}$ stacks have a mono-valence structure. Thus, the metal–insulator transition of TTF·TCNQ at 54 K[4,7] is considered to involve a $2k_f$ CDW in the mono-valence $TCNQ^{0.59-}$ stacks. The

bandwidths of the $TCNQ^{0.59-}$ and the $TTF^{0.59+}$ stacks are estimated to be 0.40 and 0.65 eV, respectively (see Table II).[11,30] Thus from eq 11, the $E_R/4$ value of TCNQ is expected to be smaller than 0.10 eV, which is substantially smaller than the corresponding value of TTF, 0.26 eV (see table II). That is, the $TTF^{0.59+}$ stack has a substantially stronger tendency for intramolecular structural localization than does the $TCNQ^{0.59-}$ stack.[30]

In contrast to TTF·TNCQ, the selenium analogue TSF·TCNQ does not exhibit a $4k_f$ CDW but only a $2k_f$ CDW.[4b,4e,32] This finding and our conclusion that the $TSF^{0.63+}$ stack prefers a mono-valence structure (see Table II) show that electrons are delocalized in the $TSF^{0.63+}$ as well as in the $TCNQ^{0.63-}$ stacks. The difference between the $TTF^{0.59+}$ and the $TSF^{0.63+}$ stacks in their preference for a mixed-valence structure stems largely from the difference in the intramolecular relaxation energies E_R of TTF and TSF. We note that a $4k_f$ CDW is also observed from the organic salts TMTTF·TCNQ and HMTTF·TCNQ,[4b] both of which contain sulfur-based donor molecules. So far, TMTSF·DMTCNQ is the only salt of a selenium-based donor that gives rise to a $4k_f$ CDW.[4b,7c] Table I reveals that, among the selenium-based donors, TMTSF has the largest $E_R/4$ values, which is close in magnitude to that of a sulfur-based donor TMTTF or HMTTF. To determine whether the $4k_f$ CDW's in those salts are due to intramolecular structural localization or electronic localization, it would be necessary to carry out XPS studies on them.

Concluding Remarks

In this work it was shown necessary to take into consideration both electronic and intramolecular structural localizations in understanding the properties of organic conducting salts. Intramolecular structural localization leads to a mixed-valence structure and hence to electron localization (i.e., formation of unpaired electrons) in the absence of strong electron correlation. Consequently, intramolecular structural localization provides a mechanism to form a $4k_f$ CDW within the small-U limit. A number of experimental observations associated with organic salts that exhibit $4k_f$ CDW's seem better described by intramolecular structural localization than by electronic localization. From the viewpoint of solid-state physics, intramolecular structural localization arises from strong electron–optical phonon (or exciton) coupling on one molecular species.[7a,33]

The intramolecular structural localization condition, $E_R/4|\beta| > 1$, derived in the present work is isomorphic to the electronic localization condition, $U/4|\beta| > 1$. Intramolecular structural localization of a molecular stack arises when the intramolecular relaxation energy E_R of the stacking molecule is large compared with $4|\beta|$. For a donor molecule, the magnitude of E_R seems to be governed by its HOMO character: An increase in the antibonding character of the HOMO leads to an increase in E_R. Given a sulfur-based donor and its selenium analogue, the former has more antibonding character. This explains why sulfur-based donors are more likely to cause intramolecular structural localization and thus a $4k_f$ CDW than are selenium-based donors. This difference between sulfur- and selenium-based donors is eventually related to the fact that selenium has a greater size and polarizability than does sulfur.[7h] Thus, both the intramolecular structural and the electronic localization conditions are less favorable for molecular stacks of selenium-based donors. Clearly, an important strategy for eliminating electron localization in molecular stacks is to select stacking molecules of small E_R value. It is noted that both TMTSF and BEDT·TTF, which form the ambient-pressure superconductors $(TMTSF)_2ClO_4$[34] and β-$(BEDT\cdot TTF)_2X$ ($X^- = I_3^-$, IBr_2^-),[35] respectively, have small E_R values (see Table I).

To exemplify the electronic and structural localizations in organic conducting salts, we have examined the band electronic structures calculated for the mono-valence and mixed-valence structures of $TTF^{1/2+}$ and $TTF^{2/3+}$ stacks. This examination led us to formulate simple structural models of $2k_f$ and $4k_f$ distortions. Either in a mono-valence or in a mixed-valence stack, electron localization is essential for the occurrence of a $4k_f$ distortion.

Acknowledgment. This work was in part supported by the Camille and Henry Dreyfus Foundation through a Teacher-Scholar Award to M.-H. W., who thanks Dr. J. P. Pouget and Dr. C. Noguera for invaluable discussions and references. S.S.S. thanks Dr. Joel Bernstein and the Organic-Metals Group at Ben-Gurion University as well as Dr. E. Canadell, Dr. O. Eisenstein, and Dr. C. Minot for stimulating discussions.

Registry No. TTF, 31366-25-3; TMTTF, 50708-37-7; HMTTF, 57512-84-2; BEDT-TTF, 66946-48-3; TTF·TCNQ, 87952-99-6; TSF·TCNQ, 100840-36-6; $(TMTSF)_2PF_6$, 73261-24-2.

Contribution from the Department of Chemistry, Michigan State University, East Lansing, Michigan 48824, AT&T Bell Laboratories, Murray Hill, New Jersey 07974, and Department of Chemistry, University of Virginia, Charlottesville, Virginia 22901

Extended X-ray Absorption Fine Structure and Powder X-ray Diffraction Study of FeOCl Intercalated with Tetrathiafulvalene and Related Molecules

S. M. Kauzlarich,[†] B. K. Teo,*[‡] and B. A. Averill*[§]

Received July 30, 1985

For FeOCl and its intercalates, $FeOCl(TTF)_{1/8.5}$ (TTF = tetrathiafulvalene), $FeOCl(TMTTF)_{1/13}$ (TMTTF = tetramethylTTF), $FeOCl(TTN)_{1/9}(toluene)_{1/23}$ (TTN = tetrathianaphthalene), and $FeOCl(TTT)_{1/9}(toluene)_{1/24}$ (TTT = tetrathiatetracene), the combination of powder X-ray diffraction data and Fe K-edge EXAFS (extended X-ray absorption fine structure) spectroscopy provides a consistent picture of the structural changes of the FeOCl host upon intercalation. On the basis of these results and the analysis of neutron diffraction data, a structural model is proposed in which the intercalant TTF is parallel to the b axis (interlayer axis) and the central C=C bond is aligned with the c axis of FeOCl. TTN and TTT are also oriented parallel to the b axis, additionally tilted at an angle $\phi \cong 30°$ (ϕ is the angle between the ac plane and the S–S bond) to accommodate the short intramolecular S–S distance of 2.10 Å. TMTTF is oriented perpendicular to the b axis.

Introduction

Structural constraints are crucial in determining the properties of low-dimensional conductors.[1-3] Compounds known as organic metals beautifully illustrate this point. This category of compounds is composed of electron donor and acceptor molecules, which when crystallized as segregated stacks are generally conductors[4,5] (σ_{RT}

[†] Michigan State University. Current address: Department of Chemistry, Iowa State University, Ames, IA 50011.
[‡] AT&T Bell Laboratories.
[§] University of Virginia.

(1) "Physics and Chemistry of Low-Dimensional Solids"; Alcacêr, L., Ed.; D. Reidel: Dordrecht, Holland, 1980.
(2) Miller, J. S.; Epstein, A. J. *Prog. Inorg. Chem.* **1976**, *20*, 1-151.
(3) Hoffman, B. M.; Ibers, J. A. *Acc. Chem. Res.* **1983**, *16*, 15-21.
(4) Green, R. L.; Street, G. B. *Science (Washington, D.C.)* **1984**, *226*, 651-656.

0020-1669/86/1325-1209$01.50/0